Ultrasonics 92 (2019) 79–92

Contents lists available at ScienceDirect

Ultrasonics

journal homepage: www.elsevier.com/locate/ultras

Aggregate gradation effects on dilatancy behavior and acoustic characteristic of cemented rockfill

Jiangyu Wu[a,b,d], Meimei Feng[a,b], Xiaoyan Ni[c], Xianbiao Mao[a,b], Zhanqing Chen[a,b], Guansheng Han[a]

[a] State Key Laboratory for Geomechanics & Deep Underground Engineering, China University of Mining & Technology, Xuzhou, Jiangsu 221116, China
[b] School of Mechanics & Civil Engineering, China University of Mining & Technology, Xuzhou, Jiangsu 221116, China
[c] School of Construction Engineering, Jiangsu Vocational Institute of Architectural Technology, Xuzhou, Jiangsu 221116, China
[d] Nottingham Centre for Geomechanics, Faculty of Engineering, University of Nottingham, University Park, Nottingham NG7 2RD, UK

ARTICLE INFO

Keywords:
Cemented rockfill
Gradation
Dilatancy
Ultrasonic
Acoustic emission

ABSTRACT

Investigating the effect of the aggregate gradation on the material properties of cemented rockfill is significant for the green mining, economic benefit and engineering safety. Consequently, the ultrasonic test, uniaxial compression experiment and acoustic emission (AE) monitor on cemented rockfill were carried out, for which the aggregate satisfied Talbot gradation. The dilatancy behavior and AE characteristic of cemented rockfill under load were investigated. The damage in the internal structure under compression was revealed by the deformation and AE signals of cemented rockfill. The effect of the Talbot index on the ultrasonic pulse velocity (UPV) and the strength parameters such as stress of dilatancy onset and uniaxial compressive strength (UCS) of cemented rockfill was analyzed. The mechanical properties of cemented rockfill materials were evaluated by the establishment of the relation between the UPV and the strength parameter. The results show that The difference between the stress of dilatancy onset and the UCS, the deformation performance and the activity of AE signals during dilatancy are positive correlated with the Talbot index of aggregate in cemented rockfill. The relation between the UPV and the strength parameters (stress of dilatancy onset and UCS) of cemented rockfill can be characterized by the positive linearity, and the UPV is also suitable for characterizing the stress of dilatancy onset of cemented rockfill material. The cubic polynomial is more suitable for describing the relations between the parameters of strength and UPV and the Talbot index of aggregate than the quadratic polynomial, and the Talbot index with optimal aggregate gradation reflected the maximum strength of cemented rockfill material should be around 0.45–0.47.

1. Introduction

Cemented rockfill is a kind of filling materials, a relatively new green material, typically uses waste rock, construction waste and other waste solid materials to crush and screen, then bonds with cementing materials and water to form [2,16,46,63]. The filling mining with cemented rockfill is a green mining technology, not only solves the waste of land resources and the pollution of water resources caused by the waste rocks in stope, but also effectively decreases the strata movement and surface subsidence during underground mining [19,56,54,55,71,88,89,87,93]. Therefore, it creates great benefits in terms of economy, environment and engineering safety.

During mining and subsequent service, the backfill structure must remain stable. Consequently, its mechanical stability is the most important quality criterion of material properties [14,31,69]. At present, the researches about the cemented filling materials mainly focus on the selection and proportioning of cementing materials and the influencing factors on its mechanical properties [66,72]. Therefore, lots of scholars studied the effects of the type and content of cementing material on the mechanical properties of cemented filling materials [1,25,62,29,30,32,82]. Due to the influence of hydration condition on the bonding process of cementing material, some researches discussed the relations between the factors such as hydration temperature, curing temperature and curing time and the mechanical properties of cemented filling materials [18,33,37,39,40,61,64,84]. In addition, other researchers found that some additives such as alkaline mineral, wood, consolidation agent, fiber and nanomaterials can promote the hydration process of cementing material. So these additive materials were appropriately mixed in the cemented filling materials to improve its mechanical properties [17,47,20,21,23,35,65,48,51,50,49]. However, the

E-mail addresses: wujiangyu@cumt.edu.cn (J. Wu), fengmeimei@cumt.edu.cn (M. Feng).

https://doi.org/10.1016/j.ultras.2018.09.008
Received 8 May 2018; Received in revised form 2 September 2018; Accepted 19 September 2018
Available online 20 September 2018
0041-624X/

Nomenclature

List of symbols

AE	acoustic emission
c	peak point
cc	initial point of elastic deformation
cd	dilatancy onset
ci	terminal point of elastic deformation
D	damage area
d	the size of particles
d_{max}	the maximum size of particles
m	mass of cementing material
M	the mass of the particles sizes below or equal to d ratio to the mass M_t of total particles mass, $M = M_t\left(\frac{d}{d_{max}}\right)^n$
M_t	the total mass of particles
$M_{d_1}^{d_2}$	the mass of particles size in the interval $[d_1, d_2]$, $M_{d_1}^{d_2} = \left[\left(\frac{d_2}{d_{max}}\right)^n - \left(\frac{d_1}{d_{max}}\right)^n\right] M_t$
n	Talbot index
o	initial point of pore compaction
P	ratio $P = \frac{M}{M_t} = \left(\frac{d}{d_{max}}\right)^n$
UCS	uniaxial compressive strength
UPV	ultrasonic pulse velocity
v	content of distilled water
XRD	X-ray diffraction
ε_1	axial strain
ε_3	circumferential strain
ε_v	volumetric strain
σ_1	axial stress
σ_{1c}	uniaxial compressive strength
σ_{1cd}	stress of dilatancy onset

above contributions on the cemented filling materials mainly focus on the strength characteristics, the dilatancy behavior is rarely investigated. In fact, from the once and again disasters in geotechnical engineering, it is easy to find that the cracks have fully developed in the internal structure of geotechnical materials before peak strength, that is, the dilatancy [75,77]. The unstable propagation of cracks in the dilatancy stage brings great hidden dangers to the engineering. As a result, it is important to explore the dilatancy behavior of cemented rockfill materials to improve the stability of backfill [53].

The cemented rockfill is a porous medium material composed of three parts of aggregate, cementing materials and pores [41]. The cementing materials have a great influence on the mechanical properties of cemented filling material [83]. However, the type, amount and obtaining method of cementing materials in actual projects are constrained by engineering conditions and engineering economic benefits [57]. For the control of pores in the backfills, it mainly depends on the filling technology in the stope and the contact difficulty between the cemented rockfill and the goaf roof [59]. At present, the cemented rockfill with the ratios of 1:2 to 1:12 are generally applied in engineering, which the ratio is the mass ratio of cementing material to aggregate [58]. That is, the aggregate accounts for at least 66% of cemented rockfill. Thus, the effect of the aggregate on the mechanical properties of cemented rockfill can't be ignored, especially for the physical and chemical properties of the aggregate and its spatial distribution in the backfills [85]. Kesimal et al. [45], Fall et al. [26] and Benzaazoua et al. [8] systematically studied the influences of the type and content of aggregate on the strength characteristics of cemented filling materials, including the early strength, late strength and long-term strength. Table 1 is the main material composition of several kinds of aggregate given by Benzaazoua et al. [8]. It believed that the strength of cemented paste backfill is negatively related to the content of sulfur in the aggregate. And it pointed out that the solid waste containing high sulfide must be desulfurized. Ke et al. [42] discussed the effect of the fineness of aggregate on the transportability and strength of cemented paste backfill. It considered that the increase in the fineness of aggregate is detrimental to the workability of cemented filling material, and its fluidity is negatively correlated with the particle fineness. However, the increase of fineness can improve the strength characteristic of cemented filling material. In contrast, Fall et al. [28] obtained the results that the medium fineness of aggregate is more conducive to the strength of cemented paste backfill. When the fine particle content reaches 35–55%, its strength remains essentially constant or begins to decrease with the decrease or increase of particle fineness. Consequently, in the effect of the aggregate distribution on the mechanical properties of cemented filling materials, the difficulty in quantifying the particle size distribution and the diversity of test conditions cause the huge differences in research results [86,4,60].

At this point, the effect of the spatial distribution of aggregate on the material properties of cemented filling material is gradually valued. Börgesson et al. [9] considered that the particle size distribution of aggregate seriously affects the homogeneity of cemented filling material, which resulted in the difference on its mechanical properties. Gautam et al. [36], Kesimal et al. [44], Sari and Pasamehmetoglu [68], and Bosiljkov [10] obtained the optimal distribution of particles in cemented filling material through experiments. As the results, the strength of cemented filling material with the optimal gradation is at least 10% higher than ungraded or other graded cemented filling material. It also improves the resistances of frost and salt [52], and with lower water requirement in cemented filling material production process [91,90]. It can be seen that the optimization on the particle size distribution of aggregate can improve the pore structure of backfill [43]. It enhances the strength characteristics of cemented rockfill by strengthening the interlaced framework structure of backfill. However, the aggregate with multiple particle sizes easily construct a high-dimensional parameter space, which greatly effects on the material properties of cemented rockfill. For example, for the aggregate with six particle size intervals of (0-d_1), (d_1-d_2), (d_2-d_3), (d_3-d_4), (d_4-d_5), and (d_5-d_6), it is necessary to seek the optimal value of the strength parameters of cemented rockfill in the six-dimensional space [Y_1:Y_2:Y_3:Y_4:Y_5:Y_6], which easily results in the curse of dimensionality [74]. Therefore, the suitable gradation function of particle size to characterize the aggregate distribution should be established, and the optimization on the distribution of particles in high-dimensional space can be obtained according to that universal function. It is really significant both in theory

Table 1
Material composition of aggregate by total dry weight (wt.%) [8].

Sample	S	Ca	Si	Al	Mg	Fe	Cu (ppm)	Zn (ppm)	Pyrite
A1	32.2	1.07	10.12	2.630	0.21	26.8	1870	45,600	60.6
A2	24.4	0.99	15.7	4.870	0.35	20.6	0.24	2.1	42.4
B	15.9	1.44	15.3	4.065	2.695	20.7	1108	1795	29.8
C	5.2	1.17	26.29	5.640	0.57	5.13	30	149	9.75

and engineering.

The filling mining technology with cemented rockfill can not only effectively solve the problems of surface subsidence, aquifer damage and groundwater resource loss caused by the fall of overlying strata in goaf, but also can prevent some hazards such as water inrush disaster formed by full development of underground watercourse and rock burst in mining process [92,94–96]. In order to ensure the filling effect and the stability of cemented rockfill under the compression of the overlying strata [78,79], the mechanical properties of cemented rockfill in stope must be evaluated [73], and the internal structures of backfills under stress must be monitored in real time [3,67].

Consequently, the ultrasonic test, uniaxial compression experiment and acoustic emission (AE) monitor on cemented rockfill were carried out, for which the aggregate satisfied Talbot gradation. The dilatancy behavior and AE characteristic of cemented rockfill under load were investigated. The damage in the internal structure under compression was revealed by the deformation and AE signals of cemented rockfill. The effect of the Talbot index on the ultrasonic pulse velocity (UPV) and the strength parameters such as stress of dilatancy onset and uniaxial compressive strength (UCS) of cemented rockfill was analyzed. The mechanical properties of cemented rockfill materials were evaluated by the establishment of the relation between the UPV and the strength parameter.

2. Experimental method

2.1. Experimental materials

In order to investigate the influence of the aggregate gradation on the material properties of cemented rockfill, it is first necessary to exclude the effect of the physical and chemical characteristics of those particles with different particle sizes. The aggregate particles with different gradations have the different specific surface areas, the particles with a higher specific surface area will release the harmful elements more easily, which accelerates the deterioration on the hydration process of cementing material. For example, the existence of sulfur causes the formations of acids and sulfates, and the acids and sulfate ions react with the hydration products such as $Ca(OH)_2$ and C-S-H to form the intumescent phases of $CaSO_4$. It causes the structure of cemented rockfill to be sparse and porous, which results in the deterioration on the backfill structure [27]. Therefore, the crushed waste rock sample with no component that can affect the hydration process of cementing material were used in this experiment, it was obtained from a coal mine in China. The cementing material is the composite Portland cement 32.5R, which is widely applied in China, due to its sufficient strength and stability [13]. Table 2 gives the primary components of the waste rock and composite Portland cement 32.5R.

2.2. Experimental specimens

For laboratory test on cemented rockfill materials, the difficulties always lie in the determination of aggregate particle size and the selection of appropriate specimen size. American Society for Testing and Materials (ASTM) [6] proposed that the minimum diameter of cylindrical specimen must exceed three times than the maximum particle size of aggregate, while Wu et al. [74] recommended to have a specimen diameter at least five times more than the largest particle size. It is to eliminate the size effect of particles in cemented rockfill specimen. In this test, the diameter of the cylindrical specimen is 50 mm, the maximum particle size of the aggregate is 10 mm.

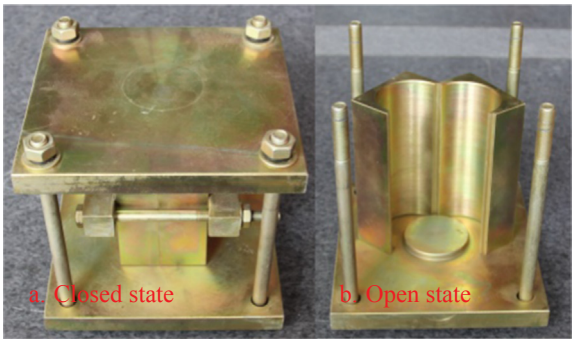

Fig. 1. Device of cemented rockfill specimen production.

In order to reduce the damage to cemented rockfill specimen during the sampling process using model [81], a device of cemented rockfill specimen production was developed [76]. The device mainly composes two halves of cylinder, an upper base, a lower base and bolts, as shown in Fig. 1. The internal diameter of cylinder is 50 mm and the internal height is 100 mm to ensure that the produced specimen is standard of $\phi 50 \times 100$, satisfied the requirements of ASTM [6]. The whole device must be clamped with the fixtures in the formation of specimen, as shown in Fig. 1a. The advantages of this device are simple and convenient, and the whole apparatus can be put into the curing equipment. During the sampling process, the cylinder can be disassembled into two parts and the specimen can be removed without damage, as shown in Fig. 1b. The release agent also cannot be applied, because the entire device was subjected to a smooth treatment and an anti-corrosion treatment.

The waste rock sample should be crushed and sieved into the specific particle size intervals of 0–0.5 mm, 0.5–1.0 mm, 1.0–1.5 mm, 1.5–2.5 mm, 2.5–5.0 mm, 5.0–8.0 and 8.0–10.0 mm. To obtain the optimal filling result, the tests on different cemented rockfill specimens made of seven types of particles with mass ratios of $Y_1{:}Y_2{:}Y_3{:}Y_4{:}Y_5{:}Y_6{:}Y_7$ are required to determine the optimal material properties of cemented rockfill in seven-dimensional space $(Y_1,Y_2,Y_3,Y_4,Y_5,Y_6{:}Y_7)$. To overcome this curse of dimensionality, it is necessary to establish a suitable universal gradation theory to describe the particle distribution. At present, the Talbot gradation theory [70] is relatively simple and convenient, and has been widely used in the fields of geomechanics and concretes. It is a continuous exponential gradation function, which can greatly quantify the effect of particle size distribution on the performance of cemented rockfill materials. Therefore, the mass ratios of the particles with seven sizes were determined by the Talbot gradation in this experiment.

The maximum size of particles is d_{max}, according to Talbot gradation, the ratio P of the mass M of particles with sizes below or equal to d to the mass M_t of total particles is:

$$P = \frac{M}{M_t} = \left(\frac{d}{d_{max}}\right)^n \tag{1}$$

Where n is the Talbot index.

The mass of particles with sizes in the interval of $[d_1, d_2]$ can be calculated according to formula (1)

Table 2
Components of waste rock and composite Portland cement 32.5R.

Varieties (%)	Al_2O_3	CaO	Fe	Fe_2O_3	K_2O	MgO	Na_2O	SiO_2	SO_3	TiO_2
Waste rock	13.21	3.91	3.69	–	0.02	2.87	–	67.75	–	–
P.C. 32.5R	4.67	62.19	–	3.69	0.68	2.87	0.21	21.56	1.91	0.16

$$M_{d_1}^{d_2} = \left[\left(\frac{d_2}{d_{\max}}\right)^n - \left(\frac{d_1}{d_{\max}}\right)^n\right] M_t \quad (2)$$

The total mass of aggregate particles in a specimen was 300 g, the mass distribution of the seven particle sizes in Talbot indices of 0.2, 0.4, 0.6 and 0.8 can be obtained according to formula (1), as shown in Table 3.

After the preparation of crushed waste rock with different particle sizes according to the Talbot gradation of Table 3, the water and cement were mixed into the crushed waste rock to form the homogeneous slurry according to the program given in Table 4. The mixed slurry poured into the device of cemented rockfill specimen production, and then the entire device must be placed on a vibratory table to vibrate to ensure the homogeneity of cemented rockfill specimen. After cement end setting, the cemented rockfill specimen should be removed and put in the curing equipment to maintain 84 days with humidity of 95% and temperature of 25 °C.

2.3. Experimental equipments

The UPV (longitudinal P-wave velocity) were measured on cemented rockfill specimens by an ultrasonic automatic cycle tester that measures the propagation of ultrasound pulses with sound amplitude accuracy of 3% and sound time accuracy of 0.5%, from Institute of Rock and Soil Mechanics, Chinese Academy of Sciences, as shown in Fig. 2. The transducers have 50 kHz, and the length of the measuring base is determined within an accuracy of 0.1 mm. The scanning speed can exceed 20 cycles/s, and the sampling interval is in (0.1, 200) μs.

The uniaxial compression tests on cemented rockfill specimens were carried out by MTS815 rock mechanics test system, which the maximum axial pressure is 4600 kN, the loading rate range is 10^{-5}-1 mm/s, the fatigue frequency is 0.001–0.5 Hz and the frame stiffness is 10.5×10^9N/m, as shown in Fig. 3. The AE21C system was used for monitoring the AE signals of cemented rockfill specimen during the loading process. The AE detectors are the piezoelectric ceramic AE sensors, the gain and threshold are 35 db, the impact time is 50 μs, the impact interval is 300 μs, and the acquisition rate is 100 ms/time. The AE signals are picked up by the detectors, which are preamplified, mainly discharged and denoised by the AE instrument to form the AE parameters (AE count, AE counting rate, energy count, energy counting rate and so on) [15].

2.4. Experimental processes

Due to the specimens were made in the rigid boundaries, the both ends were flat and smooth, and the non-parallelism and non-perpendicularity were basically controlled within ± 0.02 mm. If there are some specimens that cannot meet the test requirements, the defects must be discarded. According to ASTM Standard C597-09 [7], the UPV test on cemented rockfill specimen was first performed, the Vaseline was applied to the surfaces of transducers (transmitter and receiver) and the ends of the specimen to ensure the full contact and the elimination of the cavitation between the transducers and that test medium. It can provide the best coupling between the surface of transducer and the end of specimen to maximize the measurement accuracy. As the most satisfactory and reliable method, the direct transmission technology was used for the test where the transmitter and receiver were located on the opposite ends of cemented rockfill specimen. The UPV of the same specimen was read 5 times repeatedly, and the average value was used as the experimental result when the deviation was not great. Then the Vaseline was also daubed to the two heads of MTS to ensure the perfect coupling between the surfaces of heads and the ends of cemented rockfill specimen. According to ASTM Standard C39/C39M-15a [5], the MTS815 system was controlled to load the cemented rockfill specimen at a rate of 1 mm/min, meanwhile, the AE21C system was started to monitor the AE signals during compression.

3. Experimental results and analyses

3.1. Homogeneity and stress-strain behavior of cemented rockfill under uniaxial compression

In order to analyze the effect of the aggregate gradation on the material properties of cemented rockfill, the homogeneity of material must be discussed firstly. Fig. 4 shows the coefficient of variation on parameters such as UPV, stress of dilatancy onset and UCS of cemented rockfill with different aggregate gradations. It can be seen that the maximum coefficient of variation on UPV does not exceed 0.5%, those on stress of dilatancy onset and UCS were less than 5%. Hence, the produced cemented rockfill materials are relative homogeneous, and the dispersion among different specimens under the same condition is relative small, which can be used for investigating.

In order to discuss the mechanical properties of cemented rockfill, the stress-strain characteristic of the specimen need to be discussed firstly. For geotechnical materials, the stage of the specimen under compression can usually be divided into the following five stages. Fig. 5 shows the complete stress-strain curves of a typical cemented rockfill specimen produced whole cement.

(1) o-cc stage of Pore compaction: Under the action of axial stress, the compactions of some primary fissures and pores in the specimen causes the axial stress-axial strain curve to present a nonlinearity, while the circumferential strain remains basically unvaried, which results in the linear relation between the volumetric strain and the axial strain.

(2) cc-ci stage of Elastic deformation: Both the axial strain and the circumferential strain vary linearly in this stage, which cause a linear variation in the volumetric strain. The end point of ci in this stage is the starting point that the volumetric strain deviates from the linearity, and the relationship of $\varepsilon_1 > |\varepsilon_2 + \varepsilon_3|$ is conservative before this point.

(3) ci-cd stage of Initiation and stable expansion of cracks: Cai et al. [11] believed that the point of ci is the initiation point of crack, and the closed primary fissures, pores and new cracks in the specimen begin to open and expand after this point. The crack propagation causes a gradual increase in the circumferential strain of specimen, and the increase rate of the volumetric strain in this stage gradually decreases, which results in the deviation from linearity on that curve. Therefore, the relationship of $\varepsilon_1 > |\varepsilon_2 + \varepsilon_3|$ gradually transform to $\varepsilon_1 = |\varepsilon_2 + \varepsilon_3|$.

(4) cd-c stage of Damage and unstable propagation of cracks: When the axial stress reaches the stress of dilatancy onset at cd, the volumetric strain is the maximum value of specimen during the whole loading process, and the variation rate of the volumetric strain is zero at this second. The relationship of $\varepsilon_1 < |\varepsilon_2 + \varepsilon_3|$ is conservative after this point, thus, the volumetric strain of specimen begins to decrease, that is, the specimen transforms from compression to dilatancy. After this turning point, the irreversible damages are occurred easily in the specimen, which results in the rapid increase in the volume deformation of specimen.

(5) Failure stage: The specimen presents the strain softening characteristic after the axial stress reaches the peak. Due to the macroscopic fracture planes formed by the propagations and transfixions of cracks, the specimen can load by the frictions among the grains and the fracture planes.

Table 3
Distribution of aggregate under different Talbot indices.

n	Mass percent (%) of particles with different particle sizes (mm)						
	0–0.5	0.5–1.0	1.0–1.5	1.5–2.5	2.5–5	5.0–8.0	8.0–10.0
0.2	54.93	8.17	5.33	7.36	11.27	8.58	4.36
0.4	30.17	9.64	7.01	10.61	18.35	15.68	8.54
0.6	16.57	8.55	6.92	11.49	22.45	21.49	12.53
0.8	9.10	6.74	6.07	11.07	24.45	26.22	16.35

Table 4
Experimental program of specimens.

Specimen Number	Talbot index	Type of cementing material	Content of cementing material m (g)	Content of distilled water v (ml)	Water to cement ratio	Slump value s (mm)
1-1	0.2	Cement	60	45	0.75	151
1-2	0.4	Cement	60	45	0.75	179
1-3	0.6	Cement	60	45	0.75	187
1-4	0.8	Cement	60	45	0.75	195

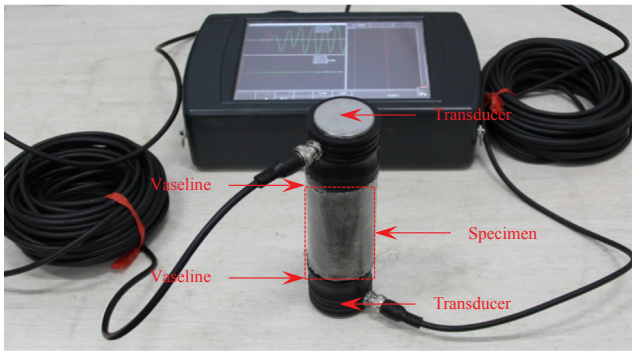

Fig. 2. Ultrasonic automatic cycle tester.

3.2. Aggregate gradation effects on dilatancy behavior and AE characteristic of cemented rockfill

Fig. 6 shows the stress-strain-AE curves of cemented rockfill specimens with different Talbot indices of aggregate. It is easy to find that the difference in dilatancy behavior among the cemented rockfill specimens with different aggregate gradations is mainly performed after the dilatancy onset. The specimen with Talbot index of 0.2 failed immediately after the dilatancy onset of cd, the abrupt decreases of circumferential strain and volumetric strain were all occurred after this specific point. And the difference between the stress of dilatancy onset and the UCS was not great, it is clearly different from the specimens with Talbot indices of 0.4, 0.6 and 0.8. Fig. 7 shows the relation between the proportional coefficient of the stress of dilatancy onset to the UCS of cemented rockfill and the Talbot index, which can be characterized by a positive linearity. It indicates that the difference between the stress of dilatancy onset and the UCS of specimen increases with Talbot index. Comparing with the specimens with different Talbot indices in Fig. 6, it is not difficult to find that the deformation performance of cemented rockfill specimen in the cd-c stage (axial strain increase of $|\varepsilon_{1c} - \varepsilon_{1cd}|$, circumferential strain and volumetric strain decreases of $|\varepsilon_{3c} - \varepsilon_{3cd}|$ and $|\varepsilon_{vc} - \varepsilon_{vcd}|$) also increases with the Talbot index.

It can be seen from Fig. 6a, the active AE signals are presented in the cemented rockfill specimen with Talbot index of 0.2 during the o-cc stage of pore compaction, which indicates that there are frequent fractures and slips among the cohesive particles in specimen during the initial loading period. The fracture-slipped cohesive particles are generally located at the bonding elements between the cement stones and the aggregate particles, thereby causing the initiation of cracks in those boundaries. It should be noted that the aggregate below 1 mm account for more than 60% of the total particles in the cemented rockfill specimen with Talbot index of 0.2. For cemented aggregate materials, on the one hand, the increase in the content of fine particles fills the pores among the coarse aggregates; on the other hand, it also increases the contact boundaries between the cement stones and the aggregate particles. Undoubtedly, the aggregate below 1 mm, which exceeds 60% of the total particles, are the direct cause of the active AE signals of this specimen in o-cc stage. It can be explained that there are more weak boundaries of cement-rock in backfill, and that too many fine particles will increase the interparticle voids [38]. This clearly differs from the specimens with Talbot indices of 0.4, 0.6, and 0.8 that exhibit relatively

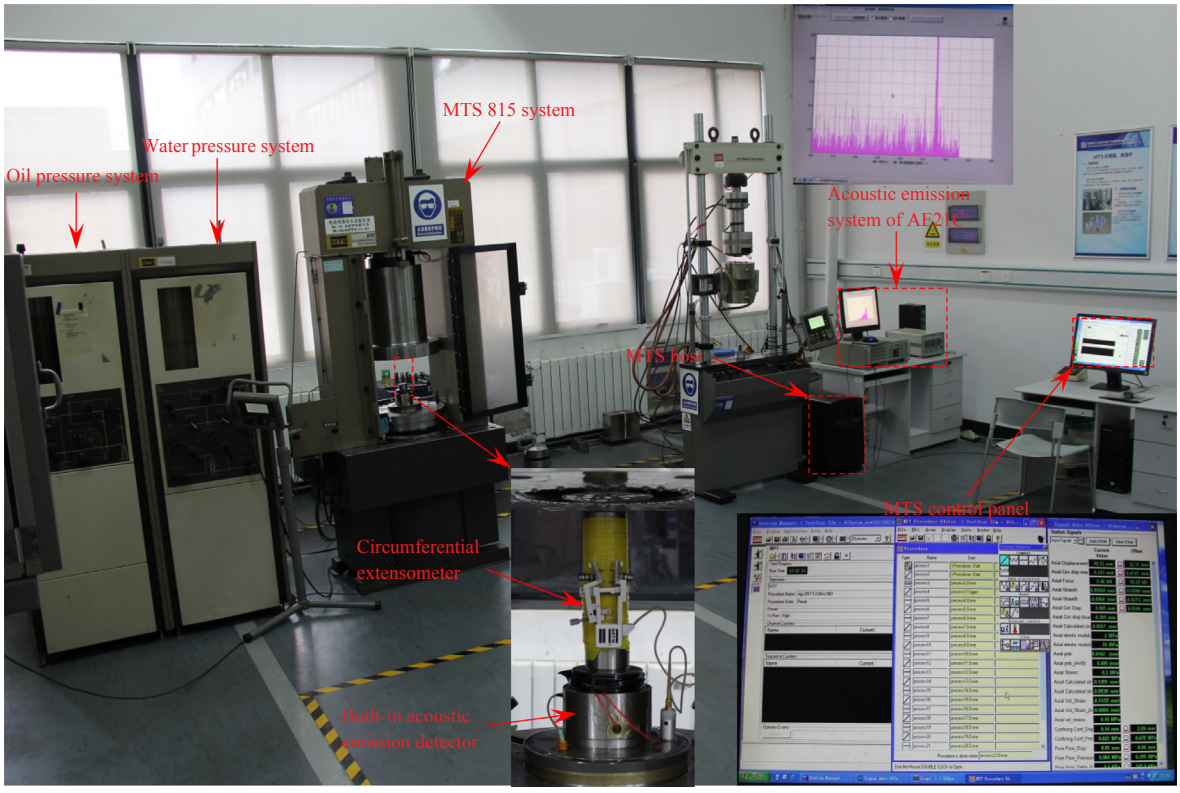

Fig. 3. Experimental systems of MTS815 and AE21C.

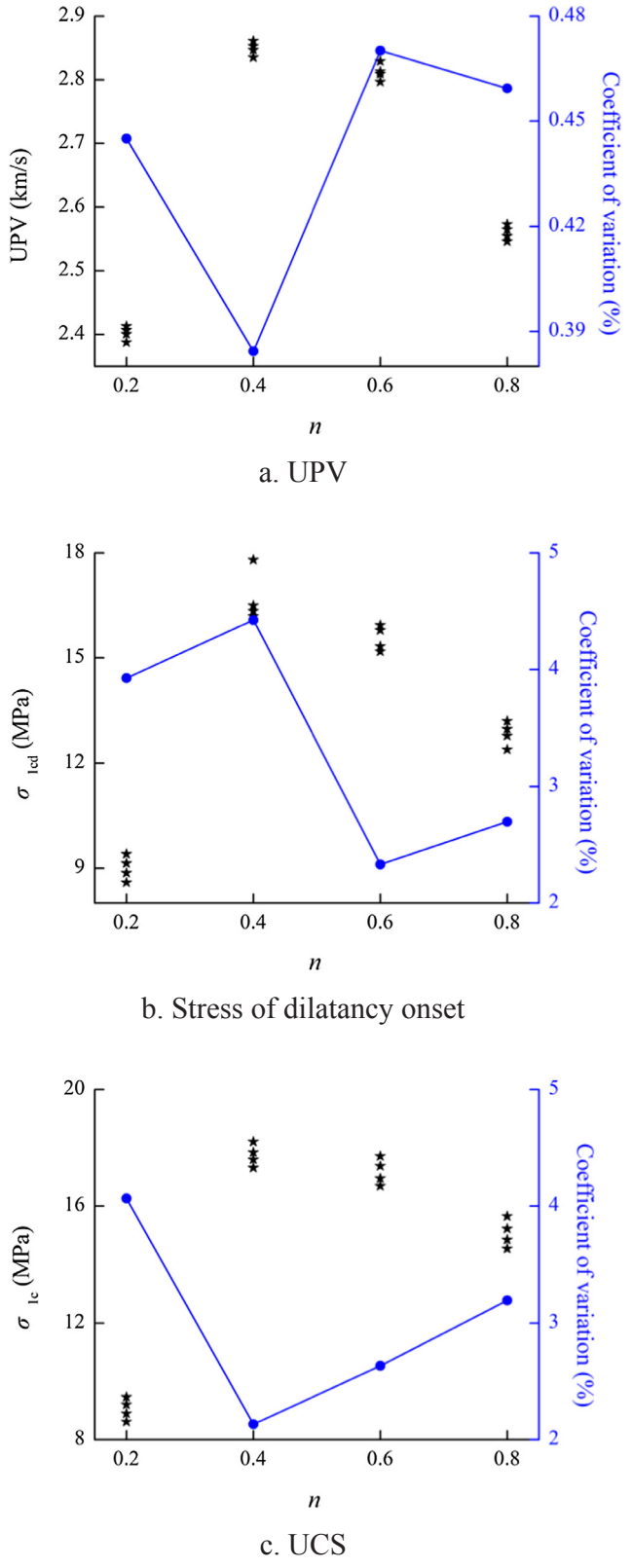

Fig. 4. Homogeneity of cemented rockfill specimens.

weak AE activity in the o-cc stage, as shown in Fig. 6b–d. In the cc-ci stage, the stress-strain behavior of cemented rockfill specimen with Talbot index of 0.2 still presents a distinct linear characteristic. The generation of AE signals can be understood as the gradual opening or even expansion of cracks that are already initiated in the structure of cemented rockfill. After the ci point, the AE signals become active again, which indicates that the evolution of cracks in the specimen starts to intensify. It greatly deteriorated the loading structure of the cemented rockfill specimen. Therefore, the difference between the dilatancy onset and the peak point is small, and the stresses of dilatancy onsets of 4 specimens with Talbot index of 0.2 are only maximum 0.06 MPa different from the UCSs.

The damage in internal structure of geo-materials can be effectively judged by the active degree of AE signals, which the criterion mechanism is consistent with the damage and failure mechanisms of geo-materials with cohesion and internal friction characteristics [34]. For the specimen with Talbot index of 0.2, it is evident that there are two damage areas labeled D, which are the o-cc stage and the ci-c stage, as shown in Fig. 6a. With the increase of the Talbot index, the damage area of the specimen mainly manifests in the ci-c stage, and the AE signals in the cd-c stage is significantly more active than the ci-cd stage, as shown in Fig. 6b–d. And the activity of AE signals is also positive correlated with the Talbot index during the dilatancy process, which is consistent with the positive relation between the deformation performance of cemented rockfill specimen and the Talbot index in the cd-c stage. Compared with the specimen with Talbot index of 0.2, the specimens with Talbot indices of 0.4, 0.6 and 0.8 can still load a certain period of time after the dilatancy onset, and will not instantaneously reach the peak to cause the unstable failure. However, it should be noted that the volumetric strain of the specimen has begun to decrease at this moment, the volume presents dilatancy deformation. And a large number of AE signals also indicate that lots of cracks non-stably propagate in specimen, which is adverse for the cemented rockfill structures. Then the cemented rockfill specimen fails after the peak point, but the structure can still load, which depends on the friction and slip among the fracture planes and the grains. The fractures and slips of cohesive particles also occur locally, which shows the frequent AE activity after the peak.

3.3. Aggregate gradation effects on strength parameters and UPV of cemented rockfill

To our knowledge, the cemented rockfill with the ratios of 1:2 to 1:12 are generally applied in engineering at present, which the ratio is the mass ratio of cementing material to aggregate. That is, the content of aggregate for the mass of cemented rockfill is at least 66% or more, thereby causing the significance in the effect of the aggregate on the cemented rockfill material. For cemented rockfill, excessive content of large aggregate tends to deteriorate the pore structure of material, which results in the formation of great voids in the structure, and the small particles cannot be completely filled. In contrast, too many fine aggregate cause the more weak boundaries of cement-rock and the increase of interparticle voids in backfill. Consequently, it is great significance to seek the optimal aggregate gradation for improving the strength of cemented rockfill or for saving the amount of filling materials, which greatly benefits to the engineering safety and economic problem. Fig. 8 shows the relation between the stress of dilatancy onset and the Talbot index. Fig. 9 presents the relation between the UCS and the Talbot index. It can be seen from the figures that the strength parameters of cemented rockfill specimen increase with the Talbot index first, and then decrease with that. The Talbot index with optimal aggregate gradation reflected the maximum strength of cemented rockfill material is between 0.4 and 0.6. Hence, the relation between the strength parameters and the Talbot index can use the polynomial function to characterize.

$$\sigma = An^3 + Bn^2 + Cn + D \tag{3}$$

$$\sigma = \alpha n^2 + \beta n + \lambda \tag{4}$$

Where σ is the strength parameter of cemented rockfill, which is used to characterize σ_{1cd} or σ_{1c}, and A, B, C, D, α, β and λ are the control

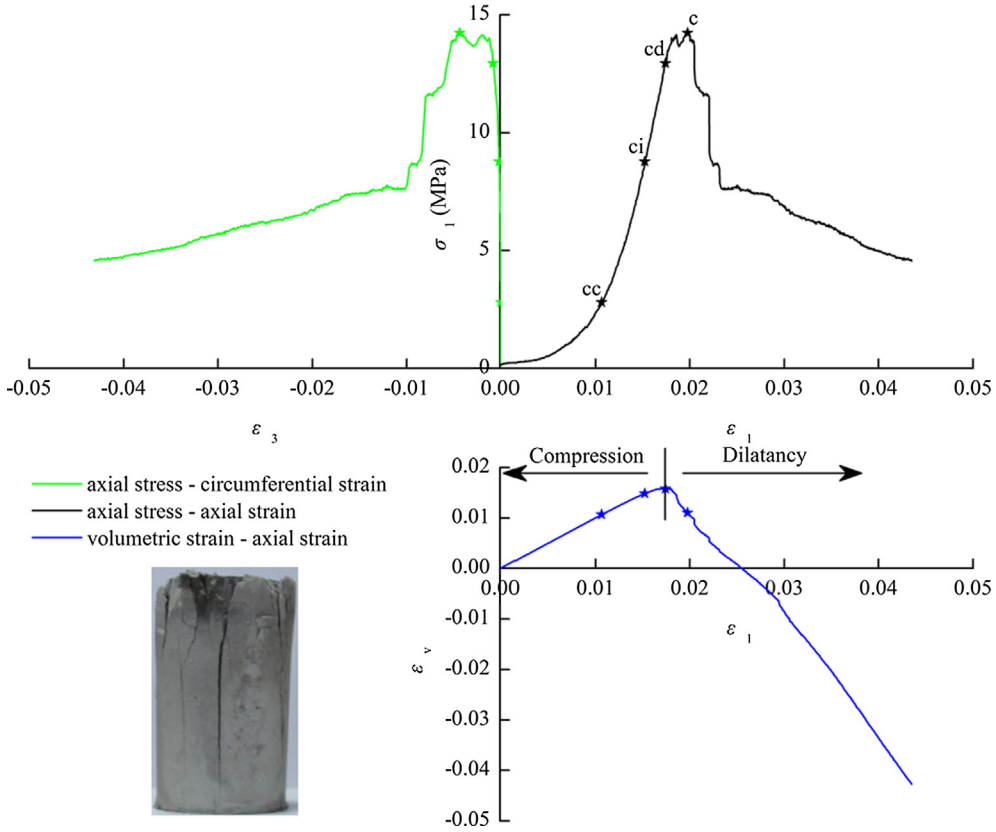

Fig. 5. Complete stress-strain curves of cemented rockfill specimen.

parameters of experimental condition.

In Figs. 8 and 9, it is easy to see that all the quadratic polynomial and the cubic polynomial can describe the relation between the strength parameters of cemented rockfill and the Talbot index of aggregate. The extremum of the functional relationship in the Talbot gradation range can be used to characterize the optimal aggregate gradation reflected the maximum strength parameters of cemented rockfill material, and the relevant parameters are given in Table 5. From the table, the Talbot index with optimal gradation obtained from the dilatancy onset is slightly lower than that based on the peak point, and the Talbot index with optimal gradation obtained from the cubic polynomial is significantly lower than that based on the quadratic polynomial. Based on the cubic polynomial function, the Talbot index with optimal aggregate gradation of cemented rockfill material should be within the range of 0.45 to 0.47, which the average values of the stress of dilatancy onset and the UCS obtained from that function are about 16.82 and 18.04 MPa. The quadratic polynomial function considers that the Talbot index with optimal aggregate gradation of cemented rockfill material should be within the range of 0.55 to 0.56, which the average values of the stress of dilatancy onset and the UCS obtained from that function are about 16.14 and 18.64 MPa.

UPV test can simply, conveniently, non-destructively, cost-effectively and accurately evaluate the intrinsic properties of geotechnical materials by using the principle of velocity measurement on ultrasonic pulse through the medium [80], thereby causing the extensive use of this technology in engineering and laboratory, which the most common application is to predict the strength parameters of geotechnical materials [22]. However, it must be established on the relation between the UPV and the strength parameters of material so as to ensure the safety and effectiveness of engineering parameters [12]. At present, there is still no systematic study on predicting the strength parameters of cemented rockfill material through UPV, especially for the cemented rockfill with the aggregate under the high-dimensional space. Thus, Fig. 10 shows the relation between the UPV of cemented rockfill specimen and the Talbot index of aggregate, and Table 6 gives the maximum UPV of cemented rockfill material characterized by the functional relationship. Therefore, that relation can also be fitted by the polynomial functions.

$$\mathrm{UPV} = En^3 + Fn^2 + Gn + H \tag{5}$$

$$\mathrm{UPV} = \delta n^2 + \omega n + \gamma \tag{6}$$

Where E, F, G, H, δ, ω and γ are the control parameters of experimental condition.

It can be seen from Fig. 10 and Table 6 that the Talbot index with optimal aggregate gradation of cemented rockfill material obtained from the cubic polynomial function is approximate 0.47, which is consistent with that optimal gradation range of 0.45–0.47 obtained from the cubic polynomial relationship between the strength parameters of cemented rockfill material and the Talbot index of aggregate. However, there is a certain gap on the Talbot index with optimal aggregate gradation of cemented rockfill material between the UPV and strength parameters. That optimal Talbot index obtained from the quadratic polynomial function based on UPV is 0.52, which is different from that optimal gradation range of 0.55–0.56 obtained from the quadratic polynomial relationship between the strength parameters of cemented rockfill material and the Talbot index of aggregate. Therefore, in the optimal gradation of cemented rockfill reflected the optimal material property through the UPV, the difference in the description of the equation also causes a certain difference. However, whether the relationship is a cubic polynomial or a quadratic polynomial, the maximum UPV of cemented rockfill material is about 2.88 km/s.

The UPV of geo-materials can reflect the intrinsic properties of materials, including the pore structure, strength and deformation properties. It is generally believed that the content of cementing material, curing temperature and curing time are positive related to the UPV of cemented rockfill material. However, about the effect of

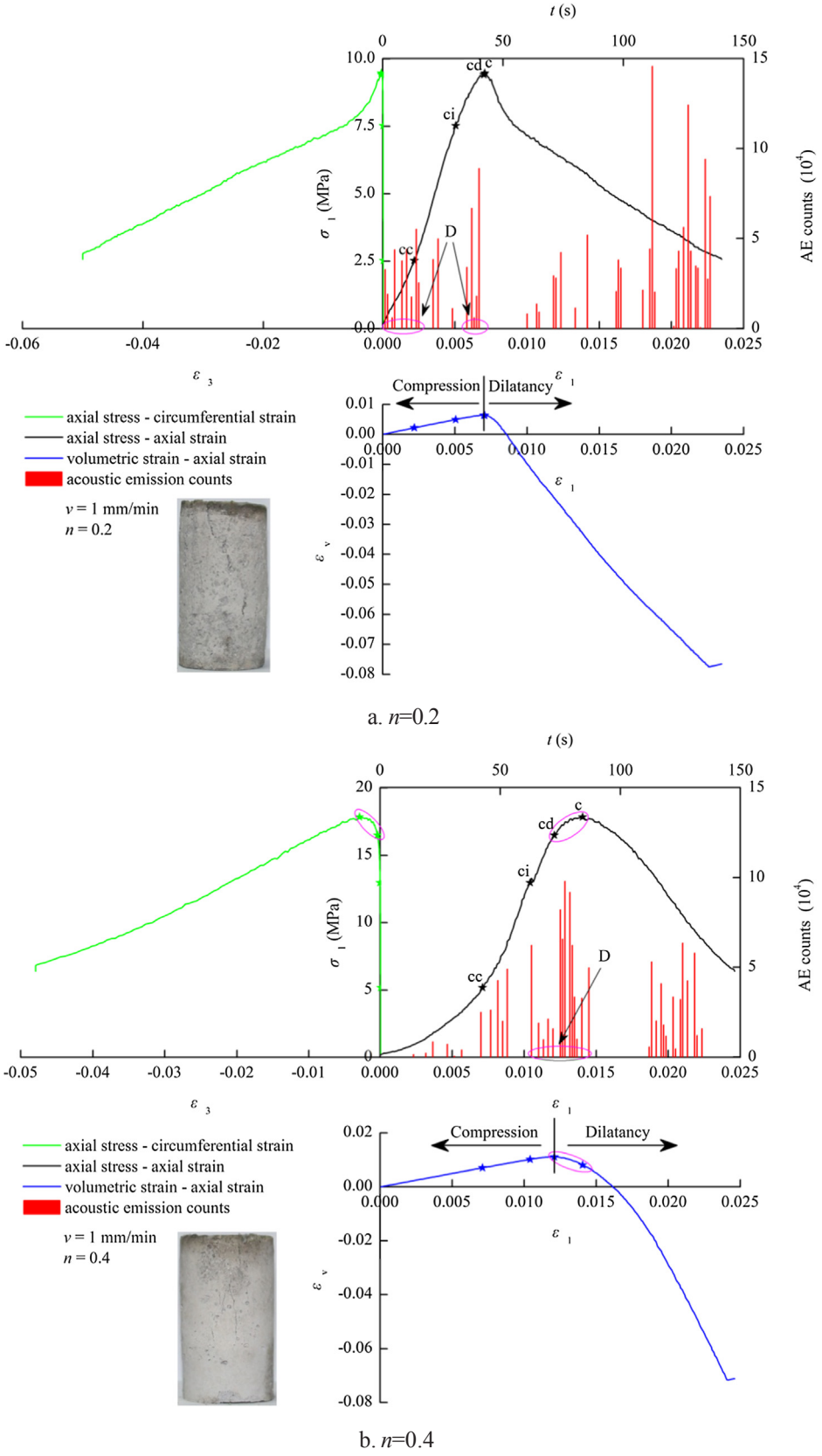

Fig. 6. Stress-strain-AE curves of cemented rockfill specimens with different Talbot indices of aggregate.

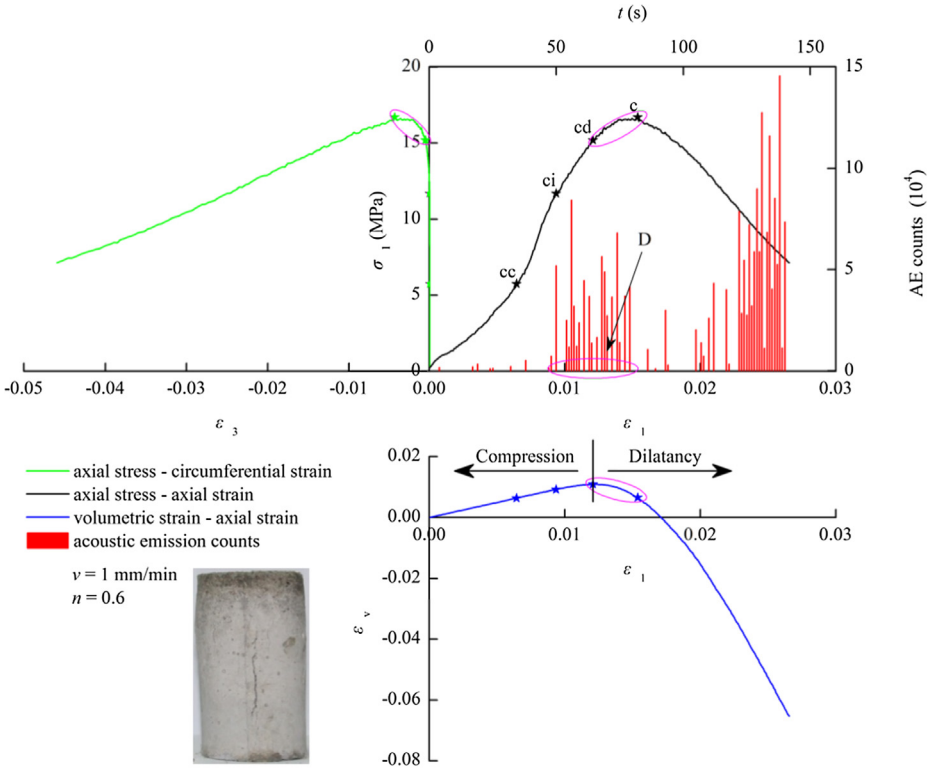

c. n=0.6

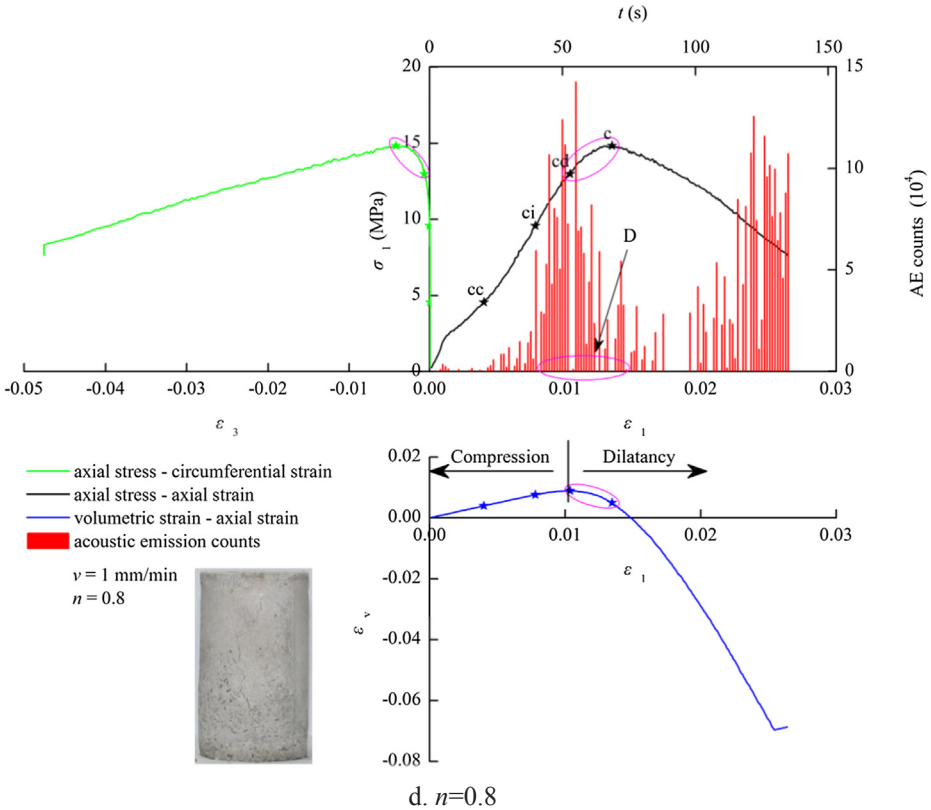

d. n=0.8

Fig. 6. (*continued*)

aggregate gradation on the UPV is rarely discussed, especially for the study on the relation between the dilatancy parameters and the UPV. In the above results, it is not difficult to find that the relation between the UPV and the Talbot index are consistent with the relation between the strength parameters and the Talbot index. Therefore, Fig. 11 shows the relationships between the strength parameters (stress of dilatancy onset and UCS) and the UPV of cemented rockfill material, which can use the positive linearity to characterize.

$$\sigma = \xi_1 \mathrm{UPV} + \xi_2 \tag{7}$$

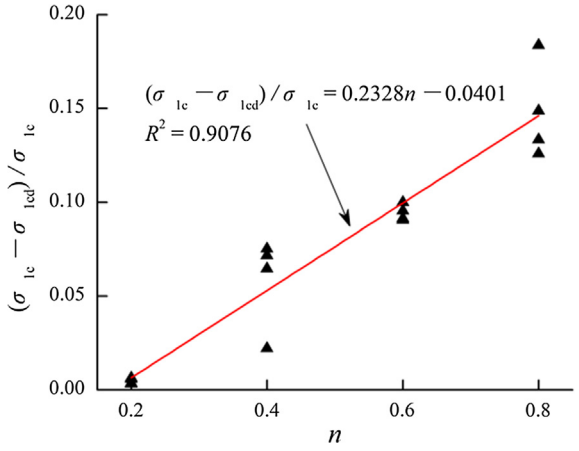

Fig. 7. Relation between proportional coefficient and Talbot index of aggregate.

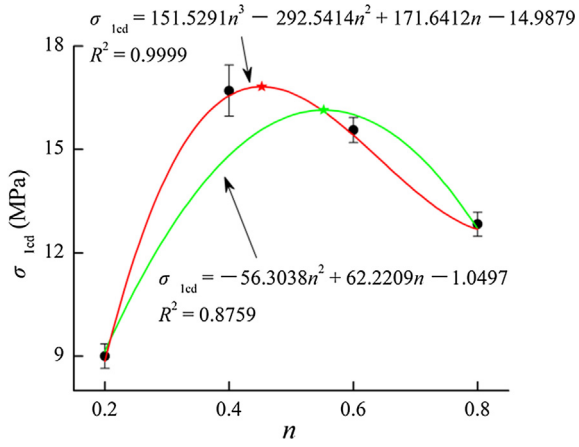

Fig. 8. Relation between stress of dilatancy onset and Talbot index of aggregate.

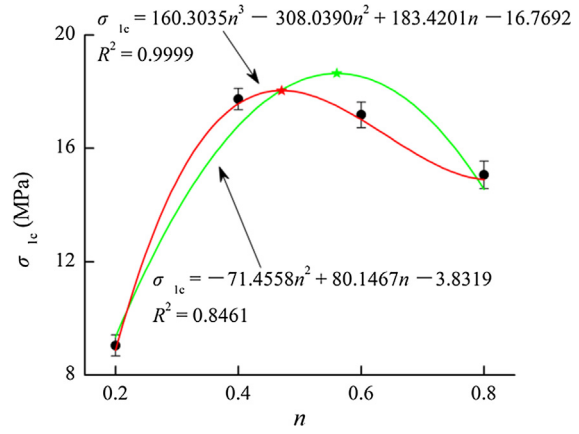

Fig. 9. Relation between UCS and Talbot index of aggregate.

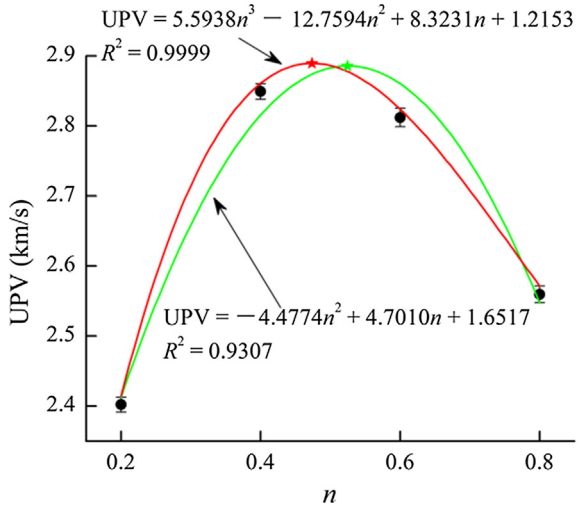

Fig. 10. Relation between UPV and Talbot index of aggregate.

Where ξ_1 and ξ_2 are the control parameters of experimental condition.

The correlation coefficient between the stress of dilatancy onset and the UPV is slight higher than that between the UCS and the UPV. This can be understood that it is caused by the effect of the difference in the spatial distribution of aggregate on the unstable propagation of cracks produced by the fractures of cohesive particles in the cement-rock boundaries of cemented rockfill material after dilatancy onset. It also shows that the UPV is suitable for characterizing the stress of dilatancy onset of cemented rockfill material, for which the aggregate satisfy the Talbot gradation.

4. Discussions

As can be seen from the results, the too fine and too coarse particle distributions cause the decreases in the strength parameters and the UPV of the cemented rockfill, which is consistent with the conclusions of Fall et al. [28] and Sari and Pasamehmetoglu [68]. In addition, Kesimal et al. [44] considered that the optimal fineness of cemented paste backfill was 25%, and its strength was larger than the specimens with the fineness less than 25% and the fineness greater than 25%. Ercikdi et al. [24] indicated that the strength of cemented paste backfill specimen with a fineness of 27.7% was significantly greater than other specimens with 16%, 49.7% and 51.0% fineness under the curing times of 28, 56, 112 and 224 days. It is summarized that the increase in the content of fine particles causes the increases in the total pores, small pores and weak boundaries of cement-rock, and the increase in the content of coarse particles causes the increase in the large pores to produce more defects, which result in the deterioration on the backfill structure to weaken its mechanical and acoustic parameters [43]. Therefore, the purpose of this paper is to evaluate the effect of the particle size distribution of aggregate on the strength parameters and UPV of cemented rockfill to obtain the optimal gradation of cemented filling materials.

Both the quadratic and cubic polynomial functions can describe the relations between the parameters of strength and UPV and the Talbot index of aggregate, which have a definite physical meaning. The

Table 5
Maximum strength parameters of cemented rockfill.

Specific point	Relationship	Correlation coefficient	n	Maximum (MPa)
Dilatancy onset	$\sigma_{1cd}=151.5291n^3-292.5414n^2+171.6412n-14.9879$	0.9999	0.4523	16.8195
	$\sigma_{1cd}=-56.3038n^2+62.2209n-1.0497$	0.8759	0.5525	16.1402
Peak point	$\sigma_{1c}=160.3035n^3-308.0390n^2+183.4201n-16.7692$	0.9999	0.4706	18.0357
	$\sigma_{1c}=-71.4558n^2+80.1467n-3.8319$	0.8461	0.5608	18.6417

Table 6
Maximum UPV of cemented rockfill.

Relationship	Correlation coefficient	n	Maximum (km/s)
UPV = $5.5938n^3 - 12.7594n^2 + 8.3231n + 1.2153$	0.9999	0.4737	2.8894
UPV = $-4.4774n^2 + 4.7010n + 1.6517$	0.9307	0.5250	2.8856

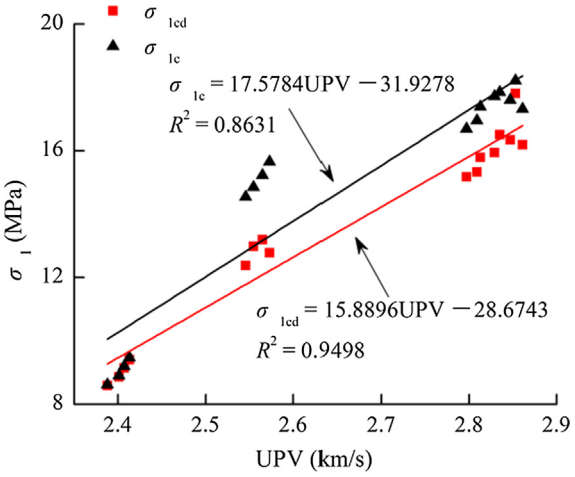

Fig. 11. Relation between strength parameters and UPV.

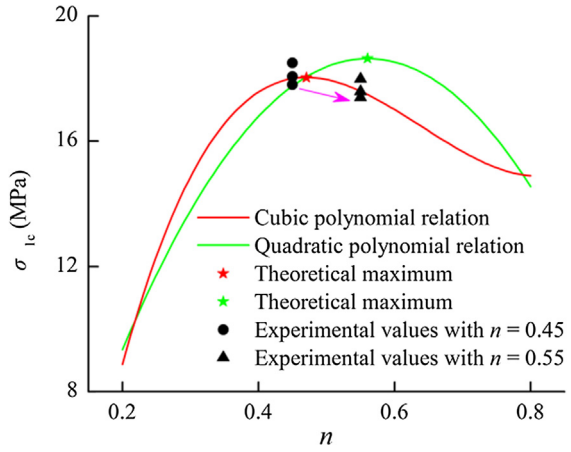

Fig. 12. UCS of cemented rockfill with the optimal aggregate gradation.

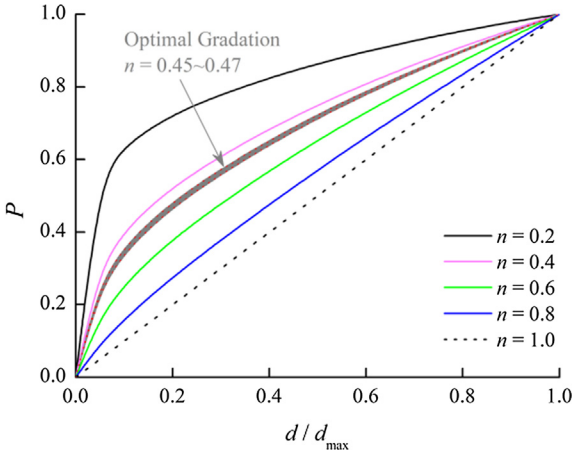

Fig. 13. Optimal aggregate gradation based on Talbot theory.

maximum calculated from that function is used to characterize the Talbot index with optimal aggregate gradation reflected the optimal material property of cemented rockfill. However, the Talbot indices with optimal aggregate gradation of cemented rockfill material obtained from the cubic polynomial function should be around 0.45 to 0.47, and those Talbot indices obtained from the quadratic polynomial function are about 0.55 to 0.56, the deviation between both is obvious. Although the correlation coefficient of cubic polynomial function on the experimental values is obviously higher than that of quadratic polynomial function, as shown in Tables 5 and 6, it is not sufficient to consider that the cubic polynomial function is more suitable for characterizing those relations than the quadratic polynomial function. Consequently, it is necessary to verify that the strength of cemented rockfill material with the optimal aggregate gradation satisfies the relationship from the essence of relation establishment. For this purpose, the total six specimens with three of 0.45 Talbot index and 0.55 Talbot index were produced under the same condition to carry out the uniaxial compression test, and the distribution of aggregate in these specimens under two conditions are given in Table 7. Fig. 12 shows the UCSs of these six specimens, it can be seen that the UCSs of cemented rockfill specimens are obvious different from the maximum obtained from the quadratic polynomial function when the Talbot index is 0.55. Moreover, the UCSs tend to decrease when the Talbot index is increased from 0.45 to 0.55. This is consistent with the cubic polynomial function but contrary to the quadratic polynomial function. Therefore, it can be concluded that the cubic polynomial function is more suitable for characterizing the relation between the strength parameters and the Talbot index of aggregate than the quadratic polynomial function, and the corresponding optimal Talbot index reflected the maximum strength of cemented rockfill material should be around 0.45 to 0.47. It is also consistent with that optimal Talbot index obtained from the UPV. And Fig. 13 gives the range of Talbot indices with optimal aggregate gradation of cemented rockfill.

5. Conclusions

The ultrasonic test, uniaxial compression experiment and AE monitor on cemented rockfill were carried out, for which the aggregate satisfied Talbot gradation. The dilatancy behavior and AE characteristic of cemented rockfill under load were investigated. The damage in the internal structure under compression was revealed by the deformation

Table 7
Distribution of aggregate under different Talbot indices.

n	Mass percent (%) of particles with different particle sizes (mm)						
	0–0.5	0.5–1.0	1.0–1.5	1.5–2.5	2.5–5	5.0–8.0	8.0–10.0
0.45	25.97	9.51	7.10	11.01	19.62	17.24	9.55
0.55	19.25	8.93	7.04	11.43	21.65	20.15	11.55

and AE signals of cemented rockfill. The effect of the Talbot index on the UPV and the strength parameters such as stress of dilatancy onset and UCS of cemented rockfill was analyzed. The mechanical properties of cemented rockfill materials were evaluated by the establishment of the relation between the UPV and the strength parameter.

(1) The difference between the stress of dilatancy onset and the UCS, the deformation performance and the activity of AE signals during dilatancy are positive correlated with the Talbot index of aggregate in cemented rockfill. With the increase of Talbot index, the two damage areas in cemented rockfill specimen characterized by AE activity transform to one damage area, which is mainly manifested in the ci-c stage. And the AE signals in the cd-c stage are more active than that in the ci-cd stage.
(2) The cemented rockfill specimen with a Talbot index of 0.2 failed immediately after the dilatancy onset, the specimens with Talbot indices of 0.4, 0.6 and 0.8 can still load a certain period of time after the dilatancy onset, and will not instantaneously reach the peak to cause the unstable failure. However, it should be noted that the volumetric strain of the specimen has begun to decrease at this moment, the volume presents dilatancy deformation. And a large number of AE signals also indicate that lots of cracks non-stably propagate in specimen, which is adverse for the cemented rockfill structures.
(3) The relation between the UPV and the strength parameters (stress of dilatancy onset and UCS) of cemented rockfill can be characterized by the positive linearity. Due to the effect of aggregate gradation on the dilatancy behavior of cemented rockfill, the correlation coefficient between the stress of dilatancy onset and the UPV is slight higher than that between the UCS and the UPV. It also shows that the UPV is suitable for characterizing the stress of dilatancy onset of cemented rockfill material, for which the aggregate satisfy the Talbot gradation.
(4) The strength parameters (stress of dilatancy onset and UCS) and UPV of cemented rockfill material increase firstly and then decrease with the increase of Talbot index, which the relation can use the polynomial function to characterize. It is considered that the cubic polynomial is more suitable for describing that relation than the quadratic polynomial, and the Talbot index with optimal aggregate gradation reflected the maximum strength of cemented rockfill material should be around 0.45–0.47.

Acknowledgments

This work was supported by the National Postdoctoral Program for Innovative Talents (BX20180359), the National Natural Science Foundation of China (51404266, 51574055) the Fundamental Research Funds for the Central Universities (2018BSCXB22, 2012LWB66) and the Postgraduate Research & Practice Innovation Program of Jiangsu Province (KYCX18_1970). The first author would like to thank Prof. Yushou Li and Prof. Qiang Zhang for the technology support and the Chinese Scholarship Council for financial support to the joint Ph. D at the University of Nottingham.

Author contributions

Wu Jiangyu, Feng Meimei, Ni Xiaoyan, Mao Xianbiao and Chen Zhanqing conceived and designed the experiments; Wu Jiangyu and Han Guansheng performed the experiments; Wu Jiangyu, Feng Meimei and Ni Xiaoyan analyzed the data; Wu Jiangyu, Feng Meimei, Ni Xiaoyan, Mao Xianbiao, Chen Zhanqing and Han Guansheng wrote the paper.

Conflict of interest

The authors declare no conflict of interest. This article does not contain any studies with human or animal subjects.

Appendix A. Supplementary material

Supplementary data to this article can be found online at https://doi.org/10.1016/j.ultras.2018.09.008.

References

[1] N. Abdul-Hussain, M. Fall, Thermo-hydro-mechanical behaviour of sodium silicate-cemented paste tailings in column experiments, Tunn. Undergr. Sp. Tech. 29 (3) (2012) 85–93.
[2] B.F. An, X.X. Miao, J.X. Zhang, F. Ju, N. Zhou, Overlying strata movement of recovering standing pillars with solid backfilling by physical simulation, Int. J. Min. Sci. Technol. 26 (2) (2016) 301–307.
[3] J.W. Archer, M.R. Dobbs, A. Aydin, H.J. Reeves, R.J. Prance, Measurement and correlation of acoustic emissions and pressure stimulated voltages in rock using an electric potential sensor, Int. J. Rock. Mech. Min. 89 (2016) 26–33.
[4] W.B. Ashraf, M.A. Noor, Laboratory-scale investigation on band gradations of aggregate for concrete, J. Mater. Civil. Eng. 25 (11) (2013) 1776–1782.
[5] ASTM Standard C39/C39M-15a, Standard test method for compressive strength of cylindrical concrete specimens, Annual Book of ASTM Standards, West Conshohocken, PA. Available online (2015), https://doi.org/10.1520/C0039_C0039M-15A.
[6] ASTM Standard C192/C192M-13a. Standard Practice for Making and Curing Concrete Test Specimens in the Lab. Annual Book of ASTM Standards, West Conshohocken, PA, 2013. Available online: https://doi.org/10.1520/C0192_C0192M-13A.
[7] ASTM Standard C597-09. Standard test method for pulse velocity through concrete. Annual Book of ASTM Standards, West Conshohocken, PA, 2009. Available online: https://doi.org/10.1520/C0597-09.
[8] M. Benzaazoua, T. Belem, B. Bussière, Chemical factors that influence the performance of mine sulphidic paste backfill, Cement. Concrete. Res. 32 (7) (2002) 1133–1144.
[9] L. Börgesson, L.E. Johannesson, D. Gunnarsson, Influence of soil structure heterogeneities on the behaviour of backfill materials based on mixtures of bentonite and crushed rock, Appl. Clay. Sci. 23 (1–4) (2003) 121–131.
[10] V.B. Bosiljkov, SCC mixes with poorly graded aggregate and high volume of limestone filler, Cement. Concrete. Res. 33 (9) (2003) 1279–1286.
[11] M. Cai, P.K. Kaiser, Y. Tasaka, T. Maejimac, H. Moriokac, M. Minami, Generalized crack initiation and crack damage stress thresholds of brittle rock masses near underground excavations, Int. J. Rock. Mech. Min. 41 (5) (2004) 833–847.
[12] S. Cao, W.D. Song, Effect of filling interval time on the mechanical strength and ultrasonic properties of cemented coarse tailing backfill, Int. J. Miner. Process. 166 (2017) 62–68.
[13] S. Cao, W.D. Song, E. Yilmaz, Influence of Structural Factors on Uniaxial Compressive Strength of Cemented Tailings Backfill, Constr. Build. Mater. 174 (2018) 190–201.
[14] S. Cao, E. Yilmaz, W.D. Song, Evaluation of viscosity, strength and microstructural properties of cemented tailings backfill, Minerals. 8 (2018) 352.
[15] A. Carpinteri, M. Corrado, G. Lacidogna, Heterogeneous materials in compression: correlations between absorbed, released and acoustic emission energies, Eng. Fail. Anal. 33 (2013) 236–250.
[16] B.S. Choudhary, S. Kumar, Underground void filling by cemented mill tailings, Int. J. Min. Sci. Technol. 23 (6) (2013) 893–900.
[17] F. Cihangir, B. Ercikdi, A. Kesimal, H. Deveci, F. Erdemir, Paste backfill of high-sulphide mill tailings using alkali-activated blast furnace slag: effect of activator nature, concentration and slag properties, Miner. Eng. 83 (2015) 117–127.
[18] F. Cihangir, B. Ercikdi, A. Kesimal, A. Turan, H. Deveci, Utilisation of alkali-activated blast furnace slag in paste backfill of high-sulphide mill tailings: effect of binder type and dosage, Miner. Eng. 30 (2012) 33–43.
[19] D.Q. Deng, L. Liu, Z.L. Yao, K. Song, D.Z. Lao, A practice of ultra-fine tailings disposal as filling material in a gold mine, J. Environ. Manage. 196 (2017) 100–109.
[20] B. Ercikdi, F. Cihangir, A. Kesimal, H. Deveci, İ. Alp, Effect of natural pozzolans as mineral admixture on the performance of cemented-paste backfill of sulphide-rich tailings, Waste Manage. Res. 28 (5) (2010) 430–435.
[21] B. Ercikdi, F. Cihangir, A. Kesimal, H. Deveci, İ. Alp, Utilization of water-reducing admixtures in cemented paste backfill of sulphide-rich mill tailings, J. Hazard. Mater. 179 (1–3) (2010) 940–946.
[22] B. Ercikdi, T. Yilmaz, G. Külekci, Strength and ultrasonic properties of cemented paste backfill, Ultrasonics. 54 (1) (2014) 195–204.
[23] B. Ercikdi, G. Külekci, T. Yılmaz, Utilization of granulated marble wastes and waste bricks as mineral admixture in cemented paste backfill of sulphide-rich tailings, Constr. Build. Mater. 93 (2015) 573–583.
[24] B. Ercikdi, H. Baki, M. İzki, Effect of desliming of sulphide-rich mill tailings on the long-term strength of cemented paste backfill, J. Environ. Manage. 115 (2013) 5–13.
[25] B. Ercikdi, A. Kesimal, F. Cihangir, H. Deveci, İ. Alp, Cemented paste backfill of sulphide-rich tailings: Importance of binder type and dosage, Cement. Concrete. Comp. 31 (4) (2009) 268–274.
[26] M. Fall, T. Belem, S. Samb, M. Benzaazoua, Experimental characterization of the stress-strain behaviour of cemented paste backfill in compression, J. Mater. Sci. 42 (11) (2007) 3914–3922.

[27] M. Fall, M. Benzaazoua, Modeling the effect of sulphate on strength development of paste backfill and binder mixture optimization, Cement. Concrete. Res. 35 (2) (2005) 301–314.
[28] M. Fall, M. Benzaazoua, S. Ouellet, Experimental characterization of the influence of tailings fineness and density on the quality of cemented paste backfill, Miner. Eng. 18 (1) (2005) 41–44.
[29] M. Fall, M. Benzaazoua, E.G. Saa, Mix proportioning of underground cemented tailings backfill, Tunn. Undergr. Sp. Tech. 23 (1) (2008) 80–90.
[30] M. Fall, J.C. Célestin, M. Pokharel, M. Touré, A contribution to understanding the effects of curing temperature on the mechanical properties of mine cemented tailings backfill, Eng. Geol. 114 (3) (2010) 397–413.
[31] M. Fall, O. Nasir, Mechanical behaviour of the interface between cemented tailings backfill and retaining structures under shear loads, Geotech. Geol. Eng. 28 (6) (2010) 779–790.
[32] M. Fall, M. Pokharel, Coupled effects of sulphate and temperature on the strength development of cemented tailings backfills: Portland cement-paste backfill, Cement. Concrete. Comp. 32 (10) (2010) 819–828.
[33] M. Fall, S.S. Samb, Effect of high temperature on strength and microstructural properties of cemented paste backfill, Fire. Saf. J. 44 (4) (2009) 642–651.
[34] X.Q. Fan, S.W. Hu, J. Lu, C.J. Wei, Acoustic emission properties of concrete on dynamic tensile test, Constr. Build. Mater. 114 (2016) 66–75.
[35] L. Festugato, A. Fourie, N.C. Consoli, Cyclic shear response of fibre-reinforced cemented paste backfill, Geotech. Lett. 3 (1) (2013) 5–12.
[36] B.P. Gautam, D.K. Panesar, S.A. Sheikh, F.J. Vecchio, Effect of coarse aggregate grading on the ASR expansion and damage of concrete, Cement. Concrete. Res. 95 (2017) 75–83.
[37] A. Ghirian, M. Fall, Coupled thermo-hydro-mechanical-chemical behaviour of cemented paste backfill in column experiments. Part II: Physical, hydraulic and thermal processes and characteristics, Eng. Geol. 164 (1) (2013) 195–207.
[38] Q.H. Guo, B.P. Xi, Z.W. Li, X.C. Zheng, J.B. Tian, H.H. Zhu, Experimental research on relationship between frequency characteristics of acoustic emission and strength parameter in concrete, J. Central South Univ.: Sci. Technol. 46 (4) (2015) 1482–1488.
[39] E. Holt, M. Leivo, Cracking risks associated with early age shrinkage, Cement. Concrete. Comp. 26 (5) (2004) 521–530.
[40] H. Jiang, M. Fall, Liang Cui, Yield stress of cemented paste backfill in sub-zero environments: Experimental results, Miner. Eng. 92 (2016) 141–150.
[41] P. Jongpradist, Effective void ratio for assessing the mechanical properties of cement-clay admixtures at high water content, J. Geotech. Geoenviron. 137 (6) (2011) 621–627.
[42] X. Ke, H. Hou, M. Zhou, Y. Wang, X. Zhou, Effect of particle gradation on properties of fresh and hardened cemented paste backfill, Constr. Build. Mater. 96 (2015) 378–382.
[43] X. Ke, X. Zhou, X.S. Wang, T. Wang, H.B. Hou, M. Zhou, Effect of tailings fineness on the pore structure development of cemented paste backfill, Constr. Build. Mater. 126 (2016) 345–350.
[44] A. Kesimal, B. Ercikdi, E. Yilmaz, The effect of desliming by sedimentation on paste backfill performance, Miner. Eng. 16 (10) (2003) 1009–1011.
[45] A. Kesimal, E. Yilmaz, B. Ercikdi, I. Alp, H. Deveci, Effect of properties of tailings and binder on the short-and long-term strength and stability of cemented paste backfill, Mater. Lett. 59 (28) (2005) 3703–3709.
[46] A. Khoshand, M. Fall, Geotechnical characterization of peat-based landfill cover materials, J. Rock Mech. Geotech. Eng. 6 (4) (2016) 1–9.
[47] B. Koohestani, T. Belem, A. Koubaa, B. Bussière, Experimental investigation into the compressive strength development of cemented paste backfill containing Nano-silica, Cement. Concrete. Comp. 72 (2016) 180–189.
[48] B. Koohestani, A. Koubaa, T. Belem, B. Bussière, H. Bouzahzah, Experimental investigation of mechanical and microstructural properties of cemented paste backfill containing maple-wood filler, Constr. Build. Mater. 121 (2016) 222–228.
[49] B. Koohestani, A.K. Darban, P. Mokhtari, A comparison between the influence of superplasticizer and organosilanes on different properties of cemented paste backfill, Constr. Build. Mater. 173 (2018) 180–188.
[50] B. Koohestani, B. Bussière, T. Belem, A. Koubaa, Influence of polymer powder on properties of cemented paste backfill, Int. J. Min. Process. 167 (2017) 1–8.
[51] B. Koohestani, Effect of saline admixtures on mechanical and microstructural properties of cementitious matrices containing tailings, Constr. Build. Mater. 156 (2017) 1019–1027.
[52] A. Lamontagne, M. Pigeon, The influence of polypropylene fibers and aggregate grading on the properties of dry-mix shotcrete, Cement. Concrete. Res. 25 (2) (1995) 293–298.
[53] L. Li, Generalized solution for mining backfill design, Int. J. Geomech. 14 (3) (2014) 613–624.
[54] M. Li, J.X. Zhang, N. Zhou, Y.L. Huang, Effect of Particle Size on the Energy Evolution of Crushed Waste Rock in Coal Mines, Rock. Mech. Rock. Eng. 50 (5) (2017) 1–8.
[55] M. Li, J.X. Zhang, Y.L. Huang, N. Zhou, Effects of particle size of crushed gangue backfill materials on surface subsidence and its application under buildings, Environ. Earth. Sci. 76 (2017) 603.
[56] X.B. Li, D.Y. Li, Z.X. Liu, G.Y. Zhao, W.H. Wang, Determination of the minimum thickness of crown pillar for safe exploitation of a subsea gold mine based on numerical modelling, Int. J. Rock. Mech. Min. 57 (1) (2013) 42–56.
[57] Z.X. Liu, W.G. Dang, Q.L. Liu, G.H. Chen, K. Peng, Optimization of clay material mixture ratio and filling process in gypsum mine goaf, Int. J. Min. Sci. Technol. 23 (3) (2013) 337–342.
[58] Z.X. Liu, X.B. Li, Study on fractal gradation of tailings and knowledge bank of its cementing strength, Chinese J. Rock Mech. Eng. 24 (10) (2005) 1789–1793.
[59] X.X. Miao, J.X. Zhang, M.M. Feng, Waste-filling in fully-mechanized coal mining and its application, J. China Univ. Min. Technol. 18 (4) (2008) 479–482.
[60] L. Orejarena, M. Fall, The use of artificial neural networks to predict the effect of sulphate attack on the strength of cemented paste backfill, B. Eng. Geol. Environ. 69 (4) (2010) 659–670.
[61] S. Ouellet, B. Bussière, M. Aubertin, M. Benzaazoua, Characterization of cemented paste backfill pore structure using Sem and Ia analysis, B. Eng. Geol. Environ. 67 (2) (2008) 139–152.
[62] S. Ouellet, B. Bussière, M. Mbonimpa, M. Benzaazoua, M. Aubertin, Reactivity and mineralogical evolution of an underground mine sulphidic cemented paste backfill, Miner. Eng. 19 (5) (2006) 407–419.
[63] N. Pajunen, G. Watkins, M. Wierink, K. Heiskanen, Drivers and barriers of effective industrial material use, Miner. Eng. 29 (2) (2012) 39–46.
[64] M. Pokharel, M. Fall, Combined influence of sulphate and temperature on the saturated hydraulic conductivity of hardened cemented paste backfill, Cement. Concrete. Comp. 38 (7) (2013) 21–28.
[65] A. Pourjavadi, S.M. Fakoorpoor, P. Hosseini, A. Khaloo, Interactions between superabsorbent polymers and cement-based composites incorporating colloidal silica nanoparticles, Cement. Concrete. Comp. 37 (1) (2013) 196–204.
[66] R.M. Rankine, N. Sivakugan, Geotechnical properties of cemented paste backfill from Cannington Mine Australia, Geotech. Geol. Eng. 25 (4) (2007) 383–393.
[67] J. Saliba, M. Matallah, A. Loukili, J. Regoin, D. Grégoire, L. Verdon, G. Pijaudier-Cabot, Experimental and numerical analysis of crack evolution in concrete through acoustic emission technique and mesoscale modelling, Eng. Fract. 167 (2016) 123–137.
[68] D. Sari, A.G. Pasamehmetoglu, The effects of gradation and admixture on the pumice lightweight aggregate concrete, Cement. Concrete. Res. 35 (5) (2005) 936–942.
[69] N. Sivakugan, R.M. Rankine, K.J. Rankine, K.S. Rankine, Geotechnical considerations in mine backfilling in Australia, J. Clean. Prod. 14 (12–13) (2006) 1168–1175.
[70] A.N. Talbot, F.E. Richart, The strength of concrete and its relation to the cement, aggregate and water, Bull., Univ. Illinois Eng. Exp. Station 137 (1923) 1–118.
[71] X.M. Wang, B. Zhao, Q.L. Zhang, Cemented backfill technology based on phosphorous gypsum, J. Cent. South Univ. Technol. 16 (2) (2009) 285–291.
[72] A.X. Wu, Y. Wang, H.J. Wang, S.H. Yin, X.X. Miao, Coupled effects of cement type and water quality on the properties of cemented paste backfill, Int. J. Miner. Process. 143 (2015) 65–71.
[73] D. Wu, Y.L. Zhang, Y.C. Liu, Mechanical performance and ultrasonic properties of cemented gangue backfill with admixture of fly ash, Ultrasonics 64 (2016) 89–96.
[74] J.Y. Wu, M.M. Feng, B.Y. Yu, Z.Q. Chen, X.B. Mao, G.S. Han, Experimental study of strength and deformation characteristics of cemented waste rock backfills with continuous gradation, Rock. Soil. Mech. 38 (1) (2017) 101–108.
[75] J.Y. Wu, M.M. Feng, B.Y. Yu, W.L. Zhang, X.Y. Ni, G.S. Han, Experimental investigation on dilatancy behavior of water-saturated sandstone, Int. J. Min. Sci. Technol. (2017), https://doi.org/10.1016/j.ijmst.2017.09.003.
[76] J.Y. Wu, M.M. Feng, Z.Q. Chen, X.B. Mao, G.S. Han, Y.M. Wang, Particle size distribution effects on the strength characteristic of cemented paste backfill, Minerals 8 (2018) 322.
[77] J.Y. Wu, M.M. Feng, B.Y. Yu, G.S. Han, The length of pre-existing fissures effects on the mechanical properties of cracked red sandstone and strength design in engineering, Ultrasonics 82 (1) (2018) 188–199.
[78] W.B. Xu, X.C. Tian, C.B. Wan, Prediction of mechanical performance of cemented paste backfill by the electrical resistivity measurement, J. Test. Eval. 46 (6) (2018) 20160183.
[79] W.B. Xu, P.W. Cao, M.M. Tian, Strength development and microstructure evolution of cemented tailings backfill containing different binder types and contents, Minerals 8 (2018) 167.
[80] E. Yilmaz, T. Belem, M. Benzaazoua, Effects of curing and stress conditions on hydromechanical, geotechnical and geochemical properties of cemented paste backfill, Eng. Geol. 168 (2) (2014) 23–37.
[81] E. Yilmaz, T. Belem, M. Benzaazoua, Specimen size effect on strength behavior of cemented paste backfills subjected to different placement conditions, Eng. Geol. 185 (2015) 52–62.
[82] E. Yilmaz, T. Belem, B. Bussière, M. Mbonimpa, Benzaazoua, M. Curing time effect on consolidation behaviour of cemented paste backfill containing different cement types and contents, Constr. Build. Mater. 75 (2015) 99–111.
[83] E. Yilmaz, M. Benzaazoua, T. Belem, B. Bussière, Effect of curing under pressure on compressive strength development of cemented paste backfill, Miner. Eng. 22 (9–10) (2009) 772–785.
[84] T. Yilmaz, B. Ercikdi, K. Karaman, G. Külekçi, Assessment of strength properties of cemented paste backfill by ultrasonic pulse velocity test, Ultrasonics. 54 (5) (2014) 1386–1394.
[85] S.H. Yin, A.X. Wu, K.J. Hu, Y. Wang, Y.K. Zhang, The effect of solid components on the rheological and mechanical properties of cemented paste backfill, Miner. Eng. 35 (6) (2012) 61–66.
[86] C.Z. Zhang, A.Q. Wang, M.S. Tang, B.Q. Wu, N.S. Zhang, Influence of aggregate size and aggregate size grading on ASR expansion, Cement. Concrete. Res. 29 (9) (1999) 1393–1396.
[87] K. Zhang, T.H. Yang, H.B. Bai, R.P. Gamage, Longwall mining-induced damage and fractures: field measurements and simulation using FDM and DEM coupled method, Int. J. Geomech. 18 (1) (2018) 04017127.
[88] J.X. Zhang, B.Y. Li, N. Zhou, Q. Zhang, Application of solid backfilling to reduce hard-roof caving and longwall coal face burst potential, Int. J. Rock. Mech. Min. 88 (2016) 197–205.
[89] J.X. Zhang, Q. Zhang, A.J.S. Spearing, X.X. Miao, S. Guo, Q. Sun, Green coal mining technique integrating mining-dressing-gas draining-backfilling-mining, Int. J. Min.

Sci. Technol. 27 (1) (2017) 17–27.
[90] T.S. Zhang, Q.J. Yu, J.X. Wei, P. Gao, P.X. Chen, J. Hu, Micro-structural development of gap-graded blended cement pastes containing a high amount of supplementary cementitious materials, Cement. Concrete. Comp. 34 (9) (2012) 1024–1032.
[91] T.S. Zhang, Q.J. Yu, J.X. Wei, P.P. Zhang, A new gap-graded particle size distribution and resulting consequences on properties of blended cement, Cement. Concrete. Comp. 33 (5) (2011) 543–550.
[92] N. Zhou, M. Li, J.X. Zhang, R. Gao, Roadway backfill method to prevent geohazards induced by room and pillar mining: a case study in Changxing coal mine, China. Nat. Hazard. Earth. Sys. 16 (12) (2016) 2473–2484.
[93] W.B. Zhu, J.M. Xu, J.L. Xu, D.Y. Chen, J.X. Shi, Pier-column backfill mining technology for controlling surface subsidence, Int. J. Rock. Mech. Min. 96 (2017) 58–65.
[94] R.C. Liu, B. Li, Y.J. Jiang, Critical hydraulic gradient for nonlinear flow through rock fracture networks: the roles of aperture, surface roughness, and number of intersections, Adv. Water. Resour. 88 (2) (2016) 53–65.
[95] R.C. Liu, B. Li, Y.J. Jiang, A fractal model based on a new governing equation of fluid flow in fractures for characterizing hydraulic properties of rock fracture networks, Comput. Geotech. 75 (5) (2016) 57–68.
[96] D. Ma, M. Rezania, H.S. Yu, H.B. Bai, Variations of hydraulic properties of granular sandstones during water inrush: Effect of small particle migration, Eng. Geol. 217 (2017) 61–70.